






**Two-band superconductivity with weak interband coupling in structurally disordered  $Y_5Rh_6Sn_{18}$** J. Juraszek <sup>1</sup>, Yu. V. Sharlai <sup>1,2</sup>, M. Konczykowski <sup>3</sup>, A. Ślebarski <sup>1</sup> and T. Cichorek <sup>1</sup><sup>1</sup>*Institute of Low Temperature and Structure Research, Polish Academy of Sciences, Wrocław 50-422, Poland*<sup>2</sup>*B. Verkin Institute for Low Temperature Physics and Engineering, Ukrainian Academy of Sciences, Kharkiv 61103, Ukraine*<sup>3</sup>*Laboratoire des Solides Irradiés, CEA/DRF/IRAMIS, École Polytechnique, CNRS, Institut Polytechnique de Paris, Palaiseau F-91128, France*

(Received 2 December 2023; revised 5 April 2024; accepted 15 April 2024; published 28 May 2024)

Temperature variation of the lower critical field  $H_{c1}(T)$  in the structurally disordered superconductor  $Y_5Rh_6Sn_{18}$  with a transition temperature  $T_c \simeq 3.2$  K was investigated using micro-Hall-probe magnetometry for local magnetization measurements. Down to about  $0.45T_c$ , an  $H_{c1}(T)$  dependence typical for a single-band  $s$ -wave BCS superconductor was observed. However, deep within the superconducting state, a sudden increase of  $H_{c1}(T)$  was found, indicating the presence of a two-band effect. By applying the two-gap  $\gamma$  model to  $Y_5Rh_6Sn_{18}$ , we revealed a very weak interband coupling in this skutterudite-related material. We speculate that the two-band superconductivity in  $Y_5Rh_6Sn_{18}$  is a base for the boosted  $T_c$  in slightly doped samples, which likely reflects a mechanism for enhancing superconductivity by disorder.

DOI: [10.1103/PhysRevB.109.174526](https://doi.org/10.1103/PhysRevB.109.174526)**I. INTRODUCTION**

Dependence of a superconducting transition temperature  $T_c$  on the concentration of nonmagnetic impurities is closely related to the momentum symmetry of the underlying gap function. This is why the  $T_c$  of an  $s$ -wave superconductor is insensitive to impurity concentration [1]. In sharp contrast, unconventional superconductivity with sign-reversing gap functions, such as  $d$ - and  $p$ -wave symmetry, is fragile in the presence of nonmagnetic impurities and structural disorder [2]. The robustness of an  $s$ -wave Cooper pair under potential disorder, however, may be weakened in a two-band superconductor with separate intraband pairing orders in each conduction band [3], as experimentally demonstrated, for example, in the first confirmed and most celebrated two-band superconductor  $MgB_2$  [4–6]. In this material the suppression of  $T_c$  is commonly explained by the averaging of the gap magnitudes between the two bands that results in the crossover from two-band to single-band superconductivity with increasing interband impurity scattering [3,7].

Recent theoretical investigations have revealed that unconventional superconducting states in multiband systems are generically less sensitive to the presence of nonmagnetic disorder compared to unconventional states in single-band materials, likely due to the spin-orbital texture of the normal-state bands [8,9]. Furthermore, enhanced stability against disorder is expected for  $s$ -wave pairing states that do not involve pairing of time-reversed partner states [8]. Additionally, both conventional and unconventional multiband superconductors are predicted to experience disorder-driven enhancements in  $T_c$  [10]. This can occur when impurity resonant states, generated by off-Fermi-level bands, lead to local density-of-states (LDOS) enhancements at the Fermi level  $E_F$  and thus, through interband coupling, impact the near-Fermi-level bands crucial for superconductivity [10]. In other

words, this so-called dilute-disorder scenario for multiband superconductors differs significantly from the effect of dense disorder in conventional one-band superconductors, where the band structure LDOS modulations can already exist in the densely disordered normal state, leading to an increase in  $T_c$  well above that of the homogeneous system [10].

Experimental evidence for enhanced superconductivity by disorder is rare. However, it has been observed for these skutterudite-related compounds  $R_5Rh_6Sn_{18}$  [11,12] ( $R = Sc$  [13,14],  $Y$  [15,16], or  $Lu$  [17]) which exhibit large static atomic displacements and local inhomogeneities on a length scale similar to the coherence length [18–21]. Among these compounds,  $Y_5Rh_6Sn_{18}$  doped with Ca demonstrates a substantial increase in  $T_c$  of up to 25% with a dopant content of less than 1.7 at. % [19]. This is accompanied by no change in crystallographic order. Moreover, doped  $Y_5Rh_6Sn_{18}$  exhibits the emergence of another phase with a critical temperature  $T_c^*$ , slightly higher than  $T_c$  of the bulk phase, but with a significantly larger disorder-driven enhancement [19]. In addition to this, the temperature dependencies of the upper critical field  $H_{c2}(T)$  and the electronic specific heat in the superconducting state of  $Y_5Rh_6Sn_{18}$  display certain features suggestive of two-band superconductivity (TBSC) [19].

In this study, we address the issue of two-band superconductivity in  $Y_5Rh_6Sn_{18}$  by examining the temperature dependence of the lower critical field  $H_{c1}(T)$ . The  $H_{c1}(T)$  behavior was inspected by means of local magnetization measurements. We employed micro-Hall-probe magnetometry, which mitigates the challenges arising from the nonellipsoidal shape of the sample under investigation. Our experimental findings demonstrate a significant enhancement of  $H_{c1}$  deep within the superconducting state of  $Y_5Rh_6Sn_{18}$ , providing strong evidence for the existence of TBSC. The disclosure of a two-band effect in this structurally disordered material holds promising implications for understanding

the mechanisms behind superconductivity enhancement by disorder.

## II. EXPERIMENT

A skutterudite-related compound  $\text{Y}_5\text{Rh}_6\text{Sn}_{18}$  crystallizes in a tetragonal structure with the space group  $I4_1/acd$  [22] corresponding to the distortion of a cubic structure of  $\text{La}_3\text{Rh}_4\text{Sn}_{13}$  type (space group  $Pm\bar{3}n$ ), which approximately doubles the length of the  $c$  axis. A polycrystalline ingot of  $\text{Y}_5\text{Rh}_6\text{Sn}_{18}$  was synthesized by arc melting technique and subsequently annealed at  $870^\circ\text{C}$  for 2 weeks, as described elsewhere [23]. We state that our sample was prepared from exactly the same ingot used earlier for the comprehensive structural, thermodynamic, and electrical transport studies presented in Ref. [23]. For the convenience of reading, the x-ray diffraction (XRD) pattern, the Rietveld refinement, and the energy-dispersive x-ray spectroscopy (EDX) results are available in the Supplemental Material [24]. They confirm a single phase of the sample used in this study and the lattice parameters  $a = 13.7601(2)$  Å and  $c = 27.5412(3)$  Å are very close to those reported for single-crystalline samples [25]. The final least-squares refinement cycle gives the weighted-profile factor  $R_{wp} = 2.7$ . While the EDX analysis indicates the good homogeneity of the sample, it also points at a small deficiency  $\delta$  of Y and a similar excess of Sn. This means that  $\text{Y}_{5-\delta}\text{Rh}_6\text{Sn}_{18+\delta}$  with  $\delta \approx 0.3$  is a real chemical composition of the sample under current investigations. We note that similar off-stoichiometry behavior was recently reported for single crystalline  $\text{Lu}_{5-\delta}\text{Rh}_6\text{Sn}_{18+\delta}$  [26].

It is worth noting that the polycrystalline samples exhibit metallic behavior with a residual resistivity ratio  $\text{RRR} = \frac{\rho(300\text{ K})}{\rho(2\text{ K})}$  of approximately 1.6; the single-crystalline samples, which contain vacancies at Y sites, display an increase of the resistivity upon cooling with  $\text{RRR} \simeq 0.8$  [25]. However, key superconducting parameters such as  $T_c$  and  $H_{c2}(0)$  as well as the  $H_{c2}(T)$  dependencies remain nearly identical between single-crystalline and polycrystalline samples.

For low-temperature magnetization measurements, we used an  $\text{Y}_5\text{Rh}_6\text{Sn}_{18}$  sample with dimensions of  $0.51 \times 0.33 \times 0.20$  mm<sup>3</sup>. The sample response to an applied magnetic field  $H$  along its shortest dimension was examined using a Hall sensor operating at temperatures as low as 0.3 K [27]. To ensure high accuracy, we applied a field-sweep rate as small as 50  $\mu\text{T}/\text{min}$ . Following each field sweep towards both the positive and negative limit, the sample was heated above  $T_c$  and then cooled again in zero applied field. In our experiments, each sensor had an active area of  $40 \times 40$   $\mu\text{m}^2$  and the middle of the sample was positioned on top of it. The Hall resistivity measured across the Hall sensor is proportional to the local magnetic induction  $B_{loc}$ . For the numerical analysis of the  $H_{c1}(T)$  profile, we used the self-consistent  $\gamma$  model elaborated by Kogan *et al.* [28] utilizing the NUMPY package [29].

## III. RESULTS

For the  $\text{Y}_5\text{Rh}_6\text{Sn}_{18}$  sample used in an  $H_{c1}$  study, we have determined its temperature dependence of the magnetization  $M(T)$  in the vicinity of superconducting transition at  $\mu_0 H = 0.02$  mT, as depicted in the upper inset of Fig. 1. A

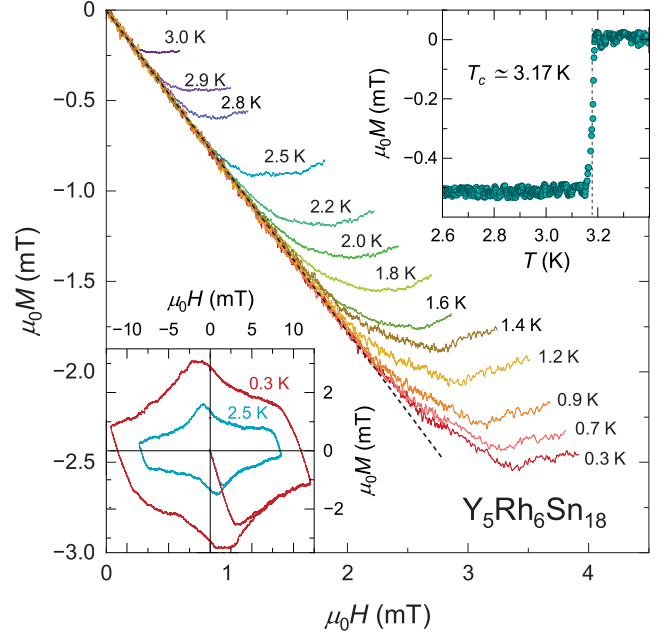


FIG. 1. Initial part of local magnetization isotherms at different temperatures down to 0.3 K for polycrystalline  $\text{Y}_5\text{Rh}_6\text{Sn}_{18}$ . The dashed line marks a shielding slope determined by a linear fit between 0 and 1.5 mT. Upper inset: the zero-field-cooling magnetization as a function of temperature measured in 0.02 mT. Lower inset:  $M$ - $H$  loops measured at 0.3 K and 2.5 K.

sharp drop of  $M(T)$  signals a narrow transition to the superconducting phase at  $T_c = 3.17(3)$  K, which is similar to that reported for single-crystalline specimens [25]. As shown in Supplemental Fig. S2, the magnetization signal remains unaffected down to the lowest temperature measured. This  $M(T)$  behavior is in full accord with the single-phase composition concluded from the aforementioned XRD and EDX results. The main panel of Fig. 1 presents the initial parts of the magnetization curves  $\mu_0 M = B_{loc} - \mu_0 H$  (where  $\mu_0 = 4\pi \times 10^{-7}$  H/m is permeability of the free space) of the  $\text{Y}_5\text{Rh}_6\text{Sn}_{18}$  sample measured using a micro-Hall-probe magnetometry at different temperatures down to 0.3 K ( $\simeq 0.09T_c$ ). The initial slope of the magnetization  $M/H = \alpha$  shows a nearly perfect linear dependence with  $\alpha = -0.89$  slightly smaller than unity. This is due to a very small but not zero distance between the active area of the Hall sensor and the sample surface which results in a magnetic field leakage around the sample edge. The lower inset of Fig. 1 compares an  $M(H)$  loop taken at 2.5 K, i.e., relatively close to  $T_c$ , with one obtained at 0.3 K, i.e., at the lowest temperature measured. The shape of both hysteresis loops taken in fields up to 12.5 mT exhibits typical type-II superconductor behavior with weak irreversibility and minor differences indicate essentially the same mechanism of weak pinning in the entire temperature range.

Figure 2 shows representative magnetic induction curves  $B(H)$  at different temperatures, obtained after removing linear term  $(1 + \alpha)\mu_0 H$  from  $B_{loc}$ . When an applied field reaches a critical value, called the field of first flux penetration  $H_p$ , the first Abrikosov vortex enters the middle of the sample and more vortices penetrate it with the further increasing magnetic

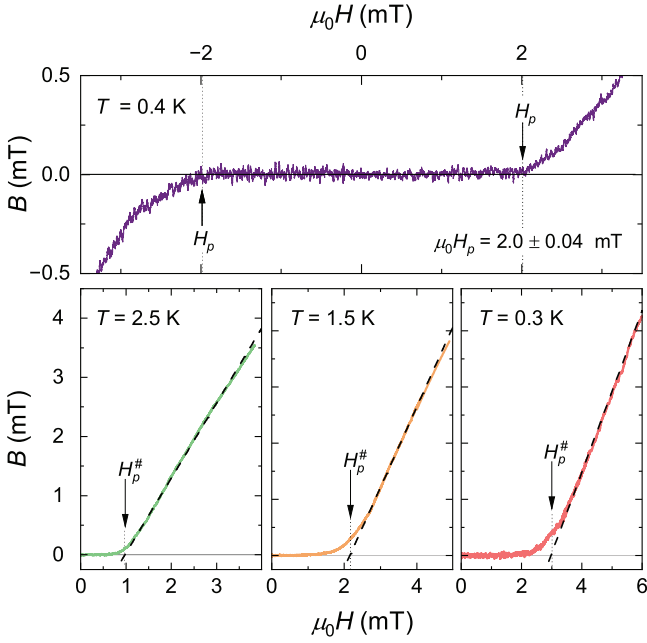


FIG. 2. Upper panel: estimation of the field of first flux penetration  $H_p$  taking the  $T = 0.4$  K data as an example. The magnetic induction ( $B$ ) versus applied field ( $H$ ) was measured for both positive and negative magnetic field sweeps. The sample was zero field cooled before each sweep. The arrows indicate  $H_p$ 's with essentially the same value for two sweeps. Lower panel: representative  $B(H)$  isotherms for increasing field showing a faster and linear increase that becomes evident above the field  $H_p^\#$  marked by the arrows.

field. Thus  $H_p$  corresponds to the field at which an increase of  $B(H)$  sets in, as indicated by black arrows. We note that although the Earth's magnetic field is not completely screened at the sample location, its impact on the  $B(H)$  isotherms can be neglected. This is illustrated by an essentially symmetric  $B(H)$  curve for the positive and negative field sweeps, as shown in the upper panel of Fig. 2. Thus the corresponding  $H_{c1}$  value at a given temperature was deduced from the average value of  $H_p = (|H_p^+| + |H_p^-|)/2$  by taking into account the geometric conversion factor. This can be calculated for a cuboid sample with dimensions  $2m \times 2n \times 2k$  using relation [30]

$$H_{c1} = \frac{H_p}{1 + \chi N}, \quad (1)$$

where  $\chi$  is the dimensionless intrinsic magnetic susceptibility of the material in the superconducting state, which can be taken to be equal to  $-1$ , and  $N = [1 + \frac{3}{4} \frac{k}{m} (1 + \frac{m}{n})]^{-1}$  stands for the effective demagnetization factor. In our experiment, the Hall sensor probes the onset of magnetic flux penetration into the sample locally; hence parameters  $2m = 40 \mu\text{m}$  and  $2n = 40 \mu\text{m}$  correspond to the width and length of the sensor active area, while parameter  $2k$  is the dimension of the sample parallel to the magnetic field. As a result, we obtained  $N = 0.12$  for the  $\text{Y}_5\text{Rh}_6\text{Sn}_{18}$  sample.

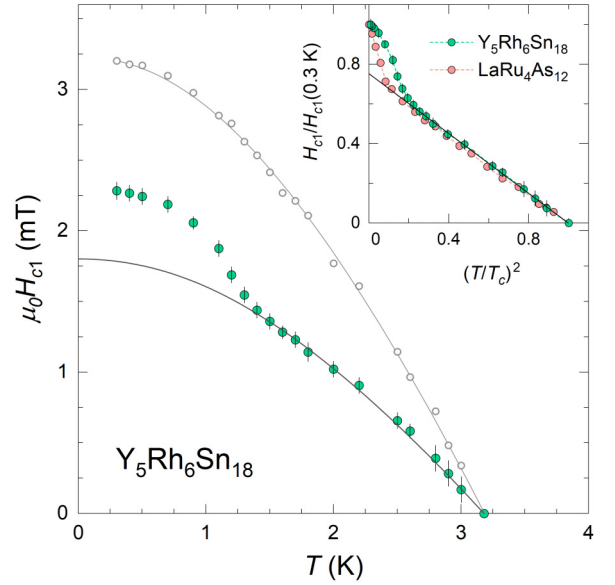


FIG. 3. Temperature dependence of the lower critical field  $H_{c1}(T)$  of polycrystalline  $\text{Y}_5\text{Rh}_6\text{Sn}_{18}$  showing a pronounced enhancement deep in the superconducting state (solid green points). Above  $T \simeq 1.4$  K, the  $H_{c1}(T)$  data follow a single-band isotropic  $s$ -wave dependence, shown by the solid black line. For comparison are also shown the  $H_p^\#$  results (open points), the temperature dependence of which is well described by the conventional BCS relation (solid gray line). Inset depicts the normalized  $H_{c1}(T)$  data of  $\text{Y}_5\text{Rh}_6\text{Sn}_{18}$  and the two-band filled-skutterudite superconductor  $\text{LaRu}_4\text{As}_{12}$  [31]. Similarly, the solid black line marks the BCS approximation.

In the Ginzburg-Landau theory, the lower critical field is given by

$$H_{c1}(T) = \frac{\phi_0}{4\pi\mu_0\lambda^2(T)} [\ln\kappa(T) + 0.5], \quad (2)$$

where  $\kappa(T) = \lambda(T)/\xi(T)$  is the Ginzburg-Landau parameter,  $\lambda(T)$  is the penetration depth, and  $\xi(T)$  is the coherence length. Since the dimensionless parameter  $\kappa(T)$  is effectively constant under the logarithm,  $H_{c1}(T)$  can be related to the normalized superfluid density as  $\tilde{\rho}_s(T) = \lambda^2(0)/\lambda^2(T) \simeq H_{c1}(T)/H_{c1}(0)$ . In other words, the behavior of  $H_{c1}(T)$  provides a powerful way to deduce the temperature dependence of the superfluid density, and hence the symmetry of underlying gap function as well as the presence of multiband effects.

Figure 3 displays the temperature dependence of  $H_{c1}$  derived for  $\text{Y}_5\text{Rh}_6\text{Sn}_{18}$  using  $B(H)$  data (cf. Fig. 2). Upon cooling down to about  $1.4$  K, the  $H_{c1}$  data show a conventional BCS-type increase. However, when the temperature decreases further, a sudden enhancement of  $H_{c1}$  emerges at around  $0.45T_c$ . At  $T = 0.3$  K, the experimental value of  $\mu_0 H_{c1}$  amounts to  $2.3(1)$  mT, which is about 25% larger than the corresponding value estimated from an extrapolation of the isotropic single-band  $s$ -wave behavior measured at higher temperatures (cf. solid black line). We emphasize that the entire  $H_{c1}(T)$  characteristic of structurally disordered  $\text{Y}_5\text{Rh}_6\text{Sn}_{18}$  is quite similar to that measured for high-quality single crystals of the filled-skutterudite two-band

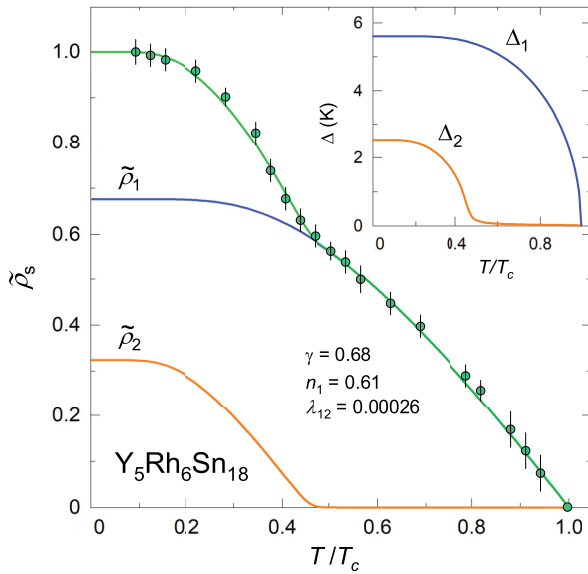


FIG. 4. Temperature dependence of the superfluid density of  $\text{Y}_5\text{Rh}_6\text{Sn}_{18}$  derived from lower-critical-field measurements using the Hall-probe magnetometry. The solid green line displays a fit to the superfluid density with an isotropic two-gap model, while the blue and orange lines show the contributions due to larger and smaller gaps, respectively. Note that the blue and green lines are indistinguishable above  $\simeq 0.45T_c$ . In this calculation, the interband coupling  $\lambda_{12} = 0.00026$  and  $\lambda_{11} = 0.40271$ ,  $\lambda_{22} = 0.52886$ ,  $n_1 = 0.61$ , and  $\gamma = 0.68$ . Inset: reduced temperature dependence of the corresponding superconducting gaps with  $\Delta_1(0)/T_c = 1.76$  and  $\Delta_2(0)/T_c = 0.79$ .

superconductor  $\text{LaRu}_4\text{As}_{12}$  ( $T_c = 10.4$  K) with  $\text{RRR} \simeq 198$  [31]. This is illustrated in the inset of Fig. 3, where the reduced  $H_{c1}$  values are plotted as a function of  $(T/T_c)^2$ .

Finally, we would like to add that the faster rise of the  $B(H)$  signal visible slightly above  $H_p$  is frequently observed in different materials and is usually ascribed to a penetration process dominated by geometrical barriers [32,33]. However, while pinning by geometrical barriers should be described by a  $\mu_0 H \sqrt{1 - (H_p/H)^2}$  law, we observe a rather linear increase above a field  $H_p^\#$ , as marked by the dashed lines in the lower panels of Fig. 2. Notwithstanding the evidence for two-band superconductivity in  $\text{Y}_5\text{Rh}_6\text{Sn}_{18}$  from the  $H_{c1}(T)$  characteristic, we note that the temperature dependence of  $H_p^\#$  does not show an enhancement at  $T \ll T_c$ . As presented in Fig. 3 (open points), the entire  $H_p^\#(T)$  behavior is well described by the conventional BCS relation. Here, the  $H_p^\#$  values were calculated with the same factor  $N = 0.12$  used above for the estimation of the  $H_{c1}$  values [cf. Eq. (1)].

#### IV. DISCUSSION

In order to gain insight into the superconducting state of  $\text{Y}_5\text{Rh}_6\text{Sn}_{18}$  we have converted the lower critical field data to the superfluid density using a relation  $\tilde{\rho}_s(T) \simeq H_{c1}(T)/H_{c1}(0)$ , where for the lower critical field at zero temperature we used  $\mu_0 H_{c1} = 2.3(1)$  mT measured at  $T = 0.3$  K. The experimental superfluid density, represented by the symbols in Fig. 4, was then fitted to  $\tilde{\rho}_s$  using a self-consistent  $\gamma$

model developed by Kogan *et al.* [28]. This model is based on a solution of the quasiclassical Eilenberger equations [34] and considers a superconductor with two bands characterized by partial densities of states  $N_1$  and  $N_2$ , where the total density of states is given by  $N(0) = N_1 + N_2$ , and two isotropic  $s$ -wave gaps  $\Delta_1$  and  $\Delta_2$  on separate sheets of the Fermi surface. Since the  $\gamma$  model [28] gives a system of nonlinear equations that must be solved numerically, we terminated the calculations when the relative error between two consecutive solutions reduces to less than  $1.5 \times 10^{-8}$ . Also, those equations include an infinite summation over the Matsubara frequencies and, accordingly, we adopted a few thousand terms of those sums.

In contrast to the widely used  $\alpha$  model, a parameter

$$\gamma = \frac{n_1 v_1^2}{n_1 v_1^2 + n_2 v_2^2} \quad (3)$$

that determines partial contributions from each band is not solely a partial density of states as in the  $\alpha$  model. Instead, it takes into account the Fermi velocities as well. Here,  $v_{1,2}^2$  are the averages over the corresponding band of the in-plane Fermi velocities and  $n_{1,2} = N_{1,2}/N(0)$ . Thus the superfluid density is  $\tilde{\rho}_s = \gamma \tilde{\rho}_1 + (1 - \gamma) \tilde{\rho}_2$ , where the partial contributions  $\tilde{\rho}_{1,2}$  are evaluated with  $\Delta_{1,2}$ . We assume the conventional electron-phonon mechanism of superconductivity and for the gap equations we use the algebraic formulas given in Refs. [28,35].

The free parameters of the model are  $\lambda_{11}$ ,  $\lambda_{22}$ ,  $\lambda_{12}$ ,  $n_1$ , and  $\gamma$ , where the dimensionless coupling constants are defined as  $\lambda_{\nu\mu} = N(0)V(\nu, \mu)$ , with  $V(\nu, \mu)$  being the effective electron-electron coupling. During the fitting, the values of these parameters are constrained to ensure that the critical temperature  $T_c$  is close to 3.2 K. Additionally, a Debye temperature of 164 K is assumed in agreement with the specific heat measurements [36]. Accordingly, both superconducting gaps were obtained self-consistently and their temperature dependencies  $\Delta_1$  and  $\Delta_2$  are shown in the inset of Fig. 4. Both order parameters are expressed in units of kelvin with  $\Delta_1(0) = 5.6$  K and  $\Delta_2(0) = 2.5$  K.

The main result of the fitting analysis is that  $\text{Y}_5\text{Rh}_6\text{Sn}_{18}$  exhibits two nearly decoupled superconducting gaps, each of which is described by the BCS relation. The interband coupling parameter is determined to be very weak and has a value of  $\lambda_{12} = 0.00026$ . This indicates that the interaction between the two bands is minimal. The obtained results and the relevant parameters are presented in Fig. 4 and Fig. S3 compares them with the corresponding fits for  $\lambda_{12} = 0.00006$  and  $\lambda_{12} = 0.00100$  (see Supplemental Material [24]). It is important to note that the long linear tail observed in the superfluid density as the temperature approaches  $T_c$  reflects the negligible contribution of the smaller gap to the total superfluid density above approximately  $0.45T_c$ . This indicates that the smaller gap has a minor influence on the overall superconducting behavior of the system above 1.5 K.

The pronounced enhancement of the superfluid density in the structurally disordered material  $\text{Y}_5\text{Rh}_6\text{Sn}_{18}$  is unexpected and intriguing. Typically, materials with substantial nonmagnetic disorder exhibit a smearing of the distinction between two-gap and single-gap behaviors due to interband impurity scattering [37–39]. The fact that  $\text{Y}_5\text{Rh}_6\text{Sn}_{18}$ , which has a



high degree of structural disorder and a small electronic mean free path compared to the coherence length [20], shows a clear two-gap anomaly in the superfluid density is remarkable. Comparisons can be made with other materials such as  $\text{MgB}_2$  and  $\text{V}_3\text{Si}$ , which are well-established two-band superconductors [37,40]. In these materials, the presence of nonmagnetic disorder has been found to result in an unexpectedly large decrease in  $T_c$  [39,41–44] and significantly affects the properties related to TBSC [45]. Interestingly, recent studies on electron-irradiated  $\text{V}_3\text{Si}$  samples with only a few pointlike defects per 1000 formula units have provided evidence for the presence of two unequal and sign-preserving gaps with the weak interband coupling  $\lambda_{12} = 0.0050$  [35]. Therefore, it is instructive to note that the structurally similar materials  $\text{Y}_5\text{Rh}_6\text{Sn}_{18}$  and  $\text{LaRu}_4\text{As}_{12}$  [27,31], but with the very different degree of structural disorder, display the normalized  $H_{c1}(T)$  dependencies which are much the same, as illustrated in the inset of Fig. 3. This indicates a robustness of a multiband  $s$ -wave superconductivity in this type of cage-forming compound. Besides, the absence of obvious anomaly in the electronic specific heat  $C_{el}$  at  $T \ll T_c$  is another parallel between both two-band superconductors with weak interband couplings [20,46]. For  $\text{LaRu}_4\text{As}_{12}$ , the detailed Fermi-surface investigation by means of de Haas–van Alphen measurements on high-quality single crystals showed that one of the bands responsible for TBSC contributes to only 4% of the DOS at  $E_F$  [47]. This explains the rather usual  $C_{el}$  behavior in the superconducting state. For  $\text{Y}_5\text{Rh}_6\text{Sn}_{18}$ , however, an experimental verification of a similar scenario appears to be challenging due to its intrinsic structural disorder [25].

Nevertheless, the  $C_{el}(T)/T$  data for another  $\text{Y}_5\text{Rh}_6\text{Sn}_{18}$  sample (different ingot) were satisfactorily described using a two-band expression with  $\Delta_1(0) = 8.7 \pm 1$  K,  $\Delta_2(0) = 3.9 \pm 1.9$  K, and assuming that the interaction between the bands is weak [19,20]. Interestingly, while that estimation of the superconducting gaps gives the larger values as those obtained from the  $H_{c1}(T)$  study (cf. Fig. 4), both experiments indicate  $\Delta_1(0)/\Delta_2(0) \approx 2.2$ .

The quasiskutterudites  $R_5\text{Rh}_6\text{Sn}_{18}$  exhibit substantial structural disorder, as confirmed by various experimental studies [18,26,48,49]. The disorder at the atomic scale is primarily caused by vacancies on the  $R$  and/or Sn sites ( $\sim 1.5$  at. %). Additionally, when an alkaline-earth metal is substituted for  $R$ , introducing local inhomogeneity on the length scale of the coherence length, the presence of another phase with a critical temperature  $T_c^*$  is observed higher than  $T_c$  for the bulk phase [19]. For instance, in  $\text{Y}_{5-x}\text{Ca}_x\text{Rh}_6\text{Sn}_{18}$  with  $x \geq 1.25$ , which can be considered as a case of dense disorder, the occurrence of another superconducting phase with  $T_c^* > T_c$  can be explained by local modulations of the crystal structure leading to enhancements in the LDOS [19]. This disorder-driven phase achieves the maximum value of  $T_c^*$  for  $x = 1.5$  and its robustness to nonmagnetic impurities can be understood with the reference to Anderson’s theorem [1]. In other words, an order parameter of the  $T_c^*$  phase appears to be of an  $s$ -wave symmetry. We note, however, that multiband effects in this phase remain an open question.

For  $\text{Y}_{5-x}\text{Ca}_x\text{Rh}_6\text{Sn}_{18}$  with  $x < 1.25$ , which corresponds to dilute disorder, the significant increase in  $T_c$  is unlikely to be associated with structural modulations as observed in the case

of dense disorder. The scanning-electron-microscope images of Ca-doped samples with less than 1.7 at. % doping show no detectable changes compared to the pure sample [19]. Additionally, the electronic band structure of  $\text{Y}_5\text{Rh}_6\text{Sn}_{18}$  does not exhibit a peak in the density of states near the Fermi level that would significantly influence the corresponding  $T_c$  through an energy shift induced by doping. This was clearly shown for the case of  $\text{Y}_5\text{Rh}_6\text{Sn}_{18}$  doped with  $\sim 1.4$  at. % of Sr, where a noticeable increase in  $T_c$  of 0.6 K is observed without substantial differences in the band structure [49]. Therefore, the anomalous  $H_{c1}(T)$  dependence observed in pure  $\text{Y}_5\text{Rh}_6\text{Sn}_{18}$  raises the question of whether the enhancement of  $T_c$  through slight alkaline-earth-metal doping can be attributed to distinct gaps on a multiband Fermi surface. This possibility aligns with the mechanism proposed by Gastiasoro and Andersen [10], which emphasizes the relevance of multiband superconductivity and impurity resonant states. In their scenario, the LDOS enhancement is generated by off-Fermi-level bands which, through interband coupling, can influence the bands crucial for superconductivity. However, in the case of  $\text{Y}_5\text{Rh}_6\text{Sn}_{18}$ , the  $H_{c1}(T)$  data clearly indicate the presence of multiple bands responsible for its superconductivity. Therefore, the mechanism of disorder-generated  $T_c$  enhancements driven by off-Fermi-level bands [10] may not be directly applicable to  $\text{Y}_{5-x}\text{Ca}_x\text{Rh}_6\text{Sn}_{18}$ . Further experimental investigations and theoretical analyses are necessary to elucidate the interplay between disorder and the enhancement of multiband superconductivity in this system.

Ending the discussion of multiband superconductivity in structurally disordered  $\text{Y}_5\text{Rh}_6\text{Sn}_{18}$ , it is important to note increasing interest in  $s$ -wave pairing states that do not pair time-reversed partner states [8]. Such exotic pairing states can arise in systems where electrons possess additional discrete degrees of freedom (DOFs). The presence of multiple internal DOFs, such as orbitals, layers, and sublattices or multiple bands opens possibilities for the internal structures of the superconducting order parameter [50]. This is a crucial aspect of the concept of superconducting fitness, which may provide a framework for describing superconductivity in complex quantum materials and enable the interpretation of seemingly contradictory experimental observations [50]. In the case of  $\text{Y}_5\text{Rh}_6\text{Sn}_{18}$ , the robustness of the two-band superconductivity against disorder and the enhanced  $T_c$  observed in Ca-substituted samples could potentially be attributed to exotic superconducting states with internal DOFs due to the intricate interplay between disorder and multiband effects.

## V. CONCLUSIONS

The experimental investigation of the lower critical field in the structurally disordered superconductor  $\text{Y}_5\text{Rh}_6\text{Sn}_{18}$  has provided valuable insights into its superconducting behavior. The measured  $H_{c1}(T)$  data revealed sudden increase in  $H_{c1}$  at approximately  $0.45T_c$ . At higher temperatures, this behavior is preceded by a typical  $H_{c1}(T)$  dependence observed in single-band  $s$ -wave BCS superconductors. Additionally, the obvious tendency to saturation of  $H_{c1}(T)$  at low temperatures indicates the presence of fully gapped superconductivity in  $\text{Y}_5\text{Rh}_6\text{Sn}_{18}$ . By employing a two-band  $\gamma$  model, the analysis of the experimental data confirmed

the existence of two distinct and essentially decoupled gaps in  $Y_5Rh_6Sn_{18}$  with an isotropic  $s$ -wave symmetry. Overall, these findings highlight the two-band superconductivity with very weak interband coupling in  $Y_5Rh_6Sn_{18}$  and suggest an interesting possibility for enhancing superconductivity by disorder-driven resonant states in slightly doped samples of this material.

## ACKNOWLEDGMENTS

This research was funded in part by the Polish NCN (National Science Centre) program for scientists from Ukraine (Grant No. R-2022/01/3/ST3/00083). We thank Vincent Mosser for contribution in design and fabrication of Hall sensors. M.K. acknowledges financial support from ANR LABEX Grant No. ANR-10-LABX-0039-PALM.

- 
- [1] P. W. Anderson, *J. Phys. Chem. Solids* **11**, 26 (1959).
- [2] A. V. Balatsky, I. Vekhter, and J.-X. Zhu, *Rev. Mod. Phys.* **78**, 373 (2006).
- [3] Y. Asano and A. Sasaki, and A. A. Golubov, *New J. Phys.* **20**, 043020 (2018).
- [4] F. Bouquet, Y. Wang, R. A. Fisher, D. G. Hinks, J. D. Jorgensen, A. Junod, and N. E. Phillips, *Europhys. Lett.* **56**, 856 (2001).
- [5] J. Kortus, I. I. Mazin, K. D. Belashchenko, V. P. Antropov, and L. L. Boyer, *Phys. Rev. Lett.* **86**, 4656 (2001).
- [6] S. L. Bud'ko, G. Lapertot, C. Petrovic, C. E. Cunningham, N. Anderson, and P. C. Canfield, *Phys. Rev. Lett.* **86**, 1877 (2001).
- [7] M. Putti, M. Affronte, C. Ferdeghini, P. Manfrinetti, C. Tarantini, and E. Lehmann, *Phys. Rev. Lett.* **96**, 077003 (2006).
- [8] D. C. Cavanagh and P. M. R. Brydon, *Phys. Rev. B* **101**, 054509 (2020).
- [9] D. C. Cavanagh and P. M. R. Brydon, *Phys. Rev. B* **104**, 014503 (2021).
- [10] M. N. Gastiasoro and B. M. Andersen, *Phys. Rev. B* **98**, 184510 (2018).
- [11] J. P. Remeika, G. P. Espinosa, A. S. Cooper, H. Barz, J. M. Rowell, D. B. McWhan, J. M. Vandenberg, D. E. Moncton, Z. Fisk, L. D. Woolf, H. C. Hamaker, M. B. Maple, G. Shirane, and W. Thomlinson, *Solid State Commun.* **34**, 923 (1980).
- [12] R. Gumeniuk, in *Handbook on the Physics and Chemistry of Rare Earths*, edited by J.-C. G. Bunzli and V. K. Pecharsky (North-Holland, Amsterdam, 2018), Vol. 54, Chap. 304, pp. 43–143.
- [13] V. Levitskiy, M. Feig, L. Akselrud, W. Schnelle, A. Leithe-Jasper, V. Dyadkin, D. Chernyshov, and R. Gumeniuk, *J. Phys.: Condens. Matter* **31**, 445603 (2019).
- [14] M. Feig, W. Schnelle, A. Maisuradze, A. Amon, Ch. Baines, M. Nicklas, S. Seiro, L. Howald, R. Khasanov, A. Leithe-Jasper, and R. Gumeniuk, *Phys. Rev. B* **102**, 024508 (2020).
- [15] N. Kase, K. Inoue, H. Hayamizu, and J. Akimitsu, *J. Phys. Soc. Jpn.* **80**, SA112 (2011).
- [16] A. Bhattacharyya, D. Adroja, N. Kase, A. Hiller, J. Akimitsu, and A. Strydom, *Sci. Rep.* **5**, 12926 (2015).
- [17] A. Bhattacharyya, D. T. Adroja, J. Quintanilla, A. D. Hillier, N. Kase, A. M. Strydom, and J. Akimitsu, *Phys. Rev. B* **91**, 060503(R) (2015).
- [18] A. Ślebarski, P. Zajdel, M. Fijałkowski, M. M. Maška, P. Witas, J. Goraus, Y. Fang, D. C. Arnold, and M. B. Maple, *New J. Phys.* **20**, 103020 (2018).
- [19] A. Ślebarski, M. Fijałkowski, P. Zajdel, M. M. Maška, J. Deniszczyk, M. Zubko, O. Pavlosiuk, K. Sasmal, and M. B. Maple, *Phys. Rev. B* **102**, 054514 (2020).
- [20] A. Ślebarski, P. Zajdel, M. M. Maška, J. Deniszczyk, and M. Fijałkowski, *J. Alloys Compd.* **819**, 152959 (2020).
- [21] A. Ślebarski and M. M. Maška, *Materials* **13**, 5830 (2020).
- [22] S. Miraglia, J. L. Hodeau, F. de Bergevin, M. Marezio, and G. P. Espinosa, *Acta Crystallogr.* **B 43**, 76 (1987).
- [23] M. Fijałkowski, M. M. Maška, J. Deniszczyk, and A. Ślebarski, *Phys. Rev. B* **104**, 165306 (2021).
- [24] See Supplemental Material at <http://link.aps.org/supplemental/10.1103/PhysRevB.109.174526> for x-ray diffraction pattern, Rietveld refinement results, results of the energy-dispersive x-ray spectroscopy analysis, and additional fits of  $\tilde{\rho}_s(T)$  with interband coupling parameters  $\lambda_{12} = 0.00006$  and  $\lambda_{12} = 0.00100$ .
- [25] Z. Zhang, Y. Xu, C. N. Kuo, X. C. Hong, M. X. Wang, P. L. Cai, J. K. Dong, C. S. Lue, and S. Y. Li, *Supercond. Sci. Technol.* **28**, 105008 (2015).
- [26] A. Wang, Z. Y. Nie, F. Du, G. M. Pang, N. Kase, J. Akimitsu, Y. Chen, M. J. Gutmann, D. T. Adroja, R. S. Perry, C. Cao, M. Smidman, and H. Q. Yuan, *Phys. Rev. B* **103**, 024503 (2021).
- [27] J. Juraszek, L. Bochenek, R. Wawryk, Z. Henkie, M. Konczykowski, and T. Cichorek, *Phys. B: Condens. Matter* **536**, 813 (2018).
- [28] V. G. Kogan, C. Martin, and R. Prozorov, *Phys. Rev. B* **80**, 014507 (2009).
- [29] C. R. Harris, K. J. Millman, S. J. van der Walt, R. Gommers, P. Virtanen, D. Cournapeau, E. Wieser, J. Taylor, S. Berg, N. J. Smith, R. Kern, M. Picus, S. Hoyer, M. H. van Kerkwijk, M. Brett, A. Haldane, J. F. del Río, M. Wiebe, P. Peterson, P. Gérard-Marchant *et al.*, *Nature (London)* **585**, 357 (2020).
- [30] K. R. Joshi, N. M. Nusran, M. A. Tanatar, K. Cho, W. R. Meier, S. L. Bud'ko, P. C. Canfield, and R. Prozorov, *Phys. Rev. Appl.* **11**, 014035 (2019).
- [31] J. Juraszek, R. Wawryk, Z. Henkie, M. Konczykowski, and T. Cichorek, *Phys. Rev. Lett.* **124**, 027001 (2020).
- [32] Z. Medvecká, T. Klein, V. Cambel, J. Šoltýs, G. Karapetrov, F. Levy-Bertrand, B. Michon, C. Marcenat, Z. Pribulová, and P. Samuely, *Phys. Rev. B* **93**, 100501(R) (2016).
- [33] E. Zeldov, A. I. Larkin, V. B. Geshkenbein, M. Konczykowski, D. Majer, B. Khaykovich, V. M. Vinokur, and H. Shtrikman, *Phys. Rev. Lett.* **73**, 1428 (1994).
- [34] G. Eilenberger, *Z. Phys.* **214**, 195 (1968).
- [35] K. Cho, M. Kończykowski, S. Ghimire, M. A. Tanatar, L.-L. Wang, V. G. Kogan, and R. Prozorov, *Phys. Rev. B* **105**, 024506 (2022).
- [36] A. Ślebarski, M. Fijałkowski, and M. M. Maška, *Phys. Rev. B* **106**, 075145 (2022).

- [37] J. Nagamatsu, N. Nakagawa, T. Muranaka, Y. Zenitani, and J. Akimitsu, *Nature (London)* **410**, 63 (2001).
- [38] E. J. Nicol and J. P. Carbotte, *Phys. Rev. B* **71**, 054501 (2005).
- [39] K. Rogacki, B. Batlogg, J. Karpinski, N. D. Zhigadlo, G. Schuck, S. M. Kazakov, P. Wägli, R. Puźniak, A. Wiśniewski, F. Carbone, A. Brinkman, and D. van der Marel, *Phys. Rev. B* **73**, 174520 (2006).
- [40] G. F. Hardy and J. K. Hulm, *Phys. Rev.* **89**, 884 (1953).
- [41] T. P. Orlando, E. J. McNiff Jr., S. Foner, and M. R. Beasley, *Phys. Rev. B* **19**, 4545 (1979).
- [42] R. Viswanathan, R. Caton, and C. S. Pande, *Phys. Rev. Lett.* **41**, 906 (1978).
- [43] J. S. Slusky, N. Rogado, K. A. Regan, M. A. Hayward, P. Khalifah, T. He, K. Inumaru, S. M. Loureiro, M. K. Haas, H. W. Zandbergen, and R. J. Cava, *Nature (London)* **410**, 343 (2001).
- [44] T. Klein, L. Lyard, J. Marcus, C. Marcenat, P. Szabó, Z. Hol'ánová, P. Samuely, B. W. Kang, H.-J. Kim, H.-S. Lee, H.-K. Lee, and S.-I. Lee, *Phys. Rev. B* **73**, 224528 (2006).
- [45] X. X. Xi, *Rep. Prog. Phys.* **71**, 116501 (2008).
- [46] L. Bochenek, R. Wawryk, Z. Henkie, and T. Cichorek, *Phys. Rev. B* **86**, 060511(R) (2012).
- [47] J. Klotz, K. Götze, V. Lorenz, Y. Prots, H. Rosner, H. Harima, L. Bochenek, Z. Henkie, T. Cichorek, I. Sheikin, and J. Wosnitzer, *Phys. Rev. B* **100**, 205106 (2019).
- [48] A. Ślebarski, M. Fijałkowski, M. M. Maška, M. Mierzejewski, B. D. White, and M. B. Maple, *Phys. Rev. B* **89**, 125111 (2014).
- [49] J. Deniszczyk and A. Ślebarski, *Materials* **15**, 2451 (2022).
- [50] A. Ramires, *J. Phys.: Condens. Matter* **34**, 304001 (2022).